RSC Advances

PAPER

View Article Online
View Journal | View Issue

Cite this: *RSC Adv.*, 2022, **12**, 7268

A MoS_2 based silver-doped ZnO nanocomposite and its antibacterial activity against β-lactamase expressing *Escherichia coli*†

Atanu Naskar, Joonho Shin and Kwang-sun Kim *

Multidrug-resistant (MDR) Gram-negative bacteria including *Escherichia coli* are increasingly resistant to current antibiotics. Among the strategies implemented to eradicate such MDR pathogens, approaches based on two-dimensional (2D) nanomaterials have received considerable attention. In particular, the excellent physicochemical properties of 2D molybdenum disulfide (MoS_2) nanosheets, including a high surface area, good conductivity, and good surface retention, are advantageous for their use as bactericidal agents. Herein, we report the fabrication of a MoS_2-based nanocomposite conjugated with silver-doped zinc oxide (AZM) as an effective antibacterial agent against *E. coli* species. The properties of AZM were characterized, and its antibacterial activity against MDR *E. coli* strains with different resistance types was evaluated. MoS_2 was found to activate the antibacterial activity of AZM and provide enhanced selectivity against MDR *E. coli* strains expressing β-lactamases. We proposed that membrane disruption of bacterial cell walls was the major cell death mechanism for MDR *E. coli*. Furthermore, surface charge perturbation could explain the differences in AZM activity against MDR *E. coli* strains expressing a β-lactamase and a mobilized colistin resistance (*mcr-1*) gene product. Thus, a MoS_2-based nanocomposite with a functional conjugation strategy could be a selective nano-antibacterial platform against infections caused by MDR *E. coli* with resistance against β-lactam antibiotics.

Received 10th January 2022
Accepted 10th February 2022

DOI: 10.1039/d2ra00163b

rsc.li/rsc-advances

1. Introduction

Multidrug-resistant (MDR) bacterial infections are "the silent tsunami facing modern medicine",[1] posing a serious threat to the global medical field. MDR bacteria, which have acquired resistance to nearly all current antibiotics, can be classified as either Gram-positive or Gram-negative bacteria. Gram-negative bacteria have a distinctive membrane structure, including an envelope and an outer membrane. These structural features prevent certain antibiotics from penetrating the cell,[2] resulting in Gram-negative bacteria being more resistant than Gram-positive bacteria.[3] Among Gram-negative bacteria, *Escherichia coli* is well known to human ecology, as it is the first bacterial species to colonize after birth.[4] Notably, *E. coli* is also a main cause of disease in nearly every part of the human body, such as gastrointestinal infections, urinary tract infections, appendicitis, meningitis, pneumonia, skin abscesses, intra-amniotic and puerperal infection in pregnant women, and endocarditis.[5] Moreover, owing to its steadily increasing resistance to antibiotics and the consequent impact on human health, *E. coli* is now included, along with the rest of the Enterobacteriaceae family, in the 'priority pathogens' list published by the World Health Organization (WHO).[6] Therefore, urgent scientific efforts are required to manage MDR *E. coli* and related infections.

Nanocomposites have been proven in many studies to have the potential to address the above problem by functioning as antibacterial agents.[7–13] The intrinsic properties of nanomaterials, such as a large surface-area-to-volume ratio, are advantageous for bacterial growth inhibition, providing a multitarget approach as compared to the single target approach of antibiotics. In particular, owing to their distinctive physiochemical properties, two-dimensional (2D) layered materials such as graphene[14,15] and black phosphorus[16,17] have emerged as promising materials for applications in areas such as biomedicine, energy, and electronics.[18,19] Molybdenum disulfide (MoS_2), another 2D nanomaterial, has also shown potential for biomedical applications, especially in terms of antibacterial activity.[15] The applicability of MoS_2 nanosheets can be attributed to their high surface area, good conductivity, and unique properties. Moreover, as MoS_2 nanosheets can induce physical damage resulting in bacterial inactivation, they are a potential antibacterial agent against Gram-negative bacterial infections.

To date, only a few studies have investigated the antibacterial activity of MoS_2 nanosheets.[20–22] Recently, MoS_2 nanosheets were shown to have rapid disinfection capabilities toward MDR *E. coli* strains and methicillin-resistant *Staphylococcus aureus*

Department of Chemistry and Chemistry Institute for Functional Materials, Pusan National University, Busan, 46241, South Korea. E-mail: kwangsun.kim@pusan.ac.kr; Fax: +82-51-516-7421; Tel: +82-51-510-2241

† Electronic supplementary information (ESI) available. See DOI: 10.1039/d2ra00163b

(MRSA) *via* a solar disinfection method.[20] In this study, the MoS_2 nanosheets were shown to have better antibacterial activity against *E. coli* than MRSA, but no selectivity toward specific types of MDR *E. coli* was observed. In another study by Ali *et al.*,[23] thiolated ligand functionalized MoS_2 nanosheets was utilized against *E. coli* and *S. aureus*, but no MDR Gram-negative bacterial strains were studied. Similar activity was observed in the work of Kasinathan *et al.*[24] where cyclodextrin functionalized multi-layered MoS_2 nanosheets were utilized against type strains of *E. coli* and *S. aureus*. Therefore, a novel approach is necessary to improve the specificity of MoS_2-based nanocomposites against MDR *E. coli* strains resistant to different antibiotics.

Doping nanoparticles can alter their physiochemical properties, such as particle size and surface area, which can play key roles in enhancing antibacterial activity.[25] For instance, a recent report showed that antibacterial activity is inversely associated with particle size.[25] Moreover, several reports showed that the properties of ZnO could be altered for various applications such as photocatalysis, sensors, and antibacterial activity by doping with metal ions.[26–29] Since Ag has been utilized as an antibacterial agent on its own, Ag doped ZnO appears to have significant potential as a new type of drug in the eradication of bacteria.[27,28] In particular, ZO and Ag are well-known for their ability to kill *E. coli*, including MDR strains.[16,25] Therefore, if MoS_2 nanosheets are decorated with ZO or Ag-doped ZO (AZO), synergistic antibacterial activity may be acquired.

Inspired by above advantageous properties and recent studies, in the present study, we successfully synthesized AZO and immobilized it on MoS_2 nanosheets (AZM) to realize the full potential of this nanocomposite material against MDR *E. coli* strains. The AZM nanocomposite was characterized using X-ray diffraction (XRD), transmission electron microscopy (TEM), and X-ray photoelectron spectroscopy (XPS). Moreover, the antibacterial activity of AZM was evaluated against MDR *E. coli* strains with different antibiotic resistance profiles. Notably, AZM was more active than ZO and AZO. Furthermore, AZM was generally more active against *E. coli* strains resistant to cell-wall-active antibiotics than to colistin-resistant. Scanning electron microscopy (SEM) and zeta potential measurements suggested that the major mode of action of AZM against MDR *E. coli* strains involved cell disruption and selective pressure strains that express cell-wall-active antibiotic-degrading enzymes (*e.g.*, β-lactamase) through surface charge perturbation. These results suggest that MoS_2 decorated with antibacterial metal oxide NPs has the potential to be used as a platform for fabricating nanoantibiotics capable of efficiently and selectively eliminating cell-wall-degrading enzyme producing MDR *E. coli* strains.

2. Materials and methods

2.1. Synthesis of AZO nanoparticles

Initially, 50 mM zinc chloride ($ZnCl_2$, 98%; Sigma-Aldrich, St. Louis, MO, USA) and 5 at% (with respect to Zn^{2+}) silver nitrate ($AgNO_3$, ≥99.9%; Sigma-Aldrich) were uniformly dispersed in a beaker containing 200 mL of deionized water with continuous stirring for 30 min at 40 °C. Subsequently, NH_4OH solution was added dropwise to the reaction mixture under continuous stirring until the pH reached 11. After stirring the mixture continuously at 90 °C for 3 h, the beaker was quickly transferred to an ice bath to stop the reaction. The precipitate was collected by centrifugation and then washed with deionized water and ethanol several times. Finally, the product was dried overnight in an air oven at 60 °C to obtain AZO nanoparticles.

2.2. Syntheses of AZM nanocomposite

MoS_2 nanosheets were prepared by the ultrasonication-assisted aqueous exfoliation of MoS_2 powder (<2 μm, 99%; Sigma-Aldrich) using a previously developed method.[30] First, 100 mg of MoS_2 was added to 20 mL of 1-methyl-2-pyrrolidinone (NMP, 99%; Sigma-Aldrich), and the resulting suspension was ultrasonicated in an ice bath ultrasonicator (to prevent overheating) for 6 h to achieve direct exfoliation. Unexfoliated MoS_2 were removed by centrifugation at 2000 rpm for 10 min, and then the supernatant was centrifuged again at 10 000 rpm for 10 min. After discarding the sediment, the directly exfoliated MoS_2 nanosheets (3.5 mg mL^{-1}) were stored in water for further use.

To prepare the AZM sample, 0.5 mL (3.5 mg mL^{-1}) of as-prepared MoS_2 nanosheets was mixed with 50 mg of as-synthesized AZO nanoparticles in 40 mL of deionized water. After ultrasonication for 10 min, the mixture was stirred continuously for 6 h. Finally, the AZM nanocomposites were collected after centrifugation and dried at 60 °C for 6 h.

2.3. Characterization

2.3.1. Material properties. The XRD patterns of as-prepared ZO, AZO, and AZM were acquired in the 2θ range of 20–80° using an X-ray diffractometer (D8 Advance with the DAVINCI design, Bruker, Billerica, MA, USA) equipped with a Ni-filtered Cu Kα radiation source (λ = 1.5406 Å). The microstructure of a representative AZM sample was evaluated using TEM (Bruker Nano GmbH). The TEM samples were prepared on carbon-coated 300 mesh Cu grids. An Axis Supra scanning XPS microprobe surface analysis system (Kratos Analytical, Manchester, UK) was used to investigate the chemical states of the elements in the representative AZM sample in the binding energy range of 200–1200 eV. The C 1s peak at 284.5 eV was employed as the binding energy reference.

2.3.2. Preparation of bacterial cells. MDR bacteria were purchased from the American Type Culture Collection (ATCC; https://www.atcc.org/), the Culture Collection of Antimicrobial Resistant Microbes (CCARM; http://knrrb.ccarm-bio.or.kr/index.jsp?rrb=ccarm), and the National Culture Collection for Pathogens (NCCP; https://nccp.kdca.go.kr/). Bacterial cells were freshly prepared using bacterial colonies grown overnight on Luria–Bertani (LB) agar plates, as described in a previous report. The cells were diluted to an optical density of 0.5 McFarland turbidity using a Sensititre™ Nephelometer (Thermo Fisher Scientific, Waltham, MA, USA). Individual cells were inoculated in Sensititre™ Cation adjusted Mueller–Hinton broth (MHB; Thermo Fisher Scientific), as described in a previous report.[7]

2.3.3. Antibacterial activity assays. The antibacterial properties of the synthesized samples were determined using

a minimal inhibitory concentration (MIC) assay, as described in a previous report.[6] The cells with 0.5 McFarland turbidity were diluted in MHB at a ratio of 1/1000. ZO, AZO, and AZM samples (5 mg mL^{-1} each) were prepared in deionized water and then serially diluted to obtain concentrations of 3.9–500 μg mL^{-1}. Then, 5 μL of each diluted sample was inoculated into 45 μL of the targeted bacterial medium. After incubating the bacterial cells by shaking at 500 rpm for 16 h at 37 °C, the MIC was determined. To differentiate the NP aggregates and grown cells, AlamarBlue™ Cell Viability Reagent (Invitrogen, CA, USA), a ready-to-use resazurin based solution that functions as a cell growth indicator by using the reducing power of living cells to quantitatively measure viability according to manufacturer's protocol. When the reagent color is changed from blue to red it indicates the bacterial growth occurred.

2.3.4. Morphological characterization of bacteria. The bacteria morphologies were characterized using SEM, as described in a previous report.[6] The SEM samples consisted of bacterial suspensions treated with AZM at sub-MICs and cultured in LB broth overnight at 37 °C with vigorous shaking.

2.3.5. Zeta potential measurements. The charges of AZM and AZM/cell mixtures at different concentrations were measured using a previously described method.[11] The reported zeta potential value for each sample is the average of triplicate measurements ± the standard deviation ($p < 0.05$).

3. Results and discussion

3.1. Material properties

3.1.1. Phase composition. The crystalline nature of the ZO, AZO, and AZM samples was analyzed using XRD analysis. As shown in Fig. 1, the XRD reflection peaks of the as-synthesized ZO, AZO, and AZM samples are perfectly indexed to hexagonal ZO (h-ZO; JCPDS 36-1451).[7] Furthermore, no silver oxide peaks were observed, confirming the sample purity. The additional peaks at approximately 39.37° and 49.60° for the AZM sample correspond to the (103) and (105) crystal planes, respectively, of few-layer MoS_2 nanosheets.[31] The average crystallite size (D) of the ZO crystallites was measured along the (101) crystal plane using the Debye–Scherrer equation:

$$D = k\lambda/\beta \cos\theta, \quad (1)$$

where k is the proportionality constant ($k = 0.89$), λ is the X-ray wavelength (1.5406 Å), β is the full width at half maximum for the peak of maximum intensity (in radians), θ is the diffraction angle, and D is the crystallite size.

The D values calculated for ZO, AZO, and AZM were approximately 25, 21, and 21 nm, respectively. The reduction of

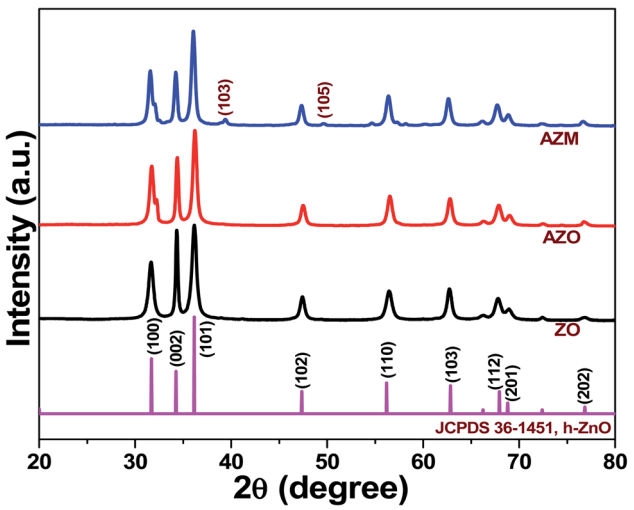

Fig. 1 X-ray diffraction (XRD) patterns of ZnO (ZO), Ag-doped ZnO (AZO), and Ag-doped ZnO/MoS_2 (AZM) samples.

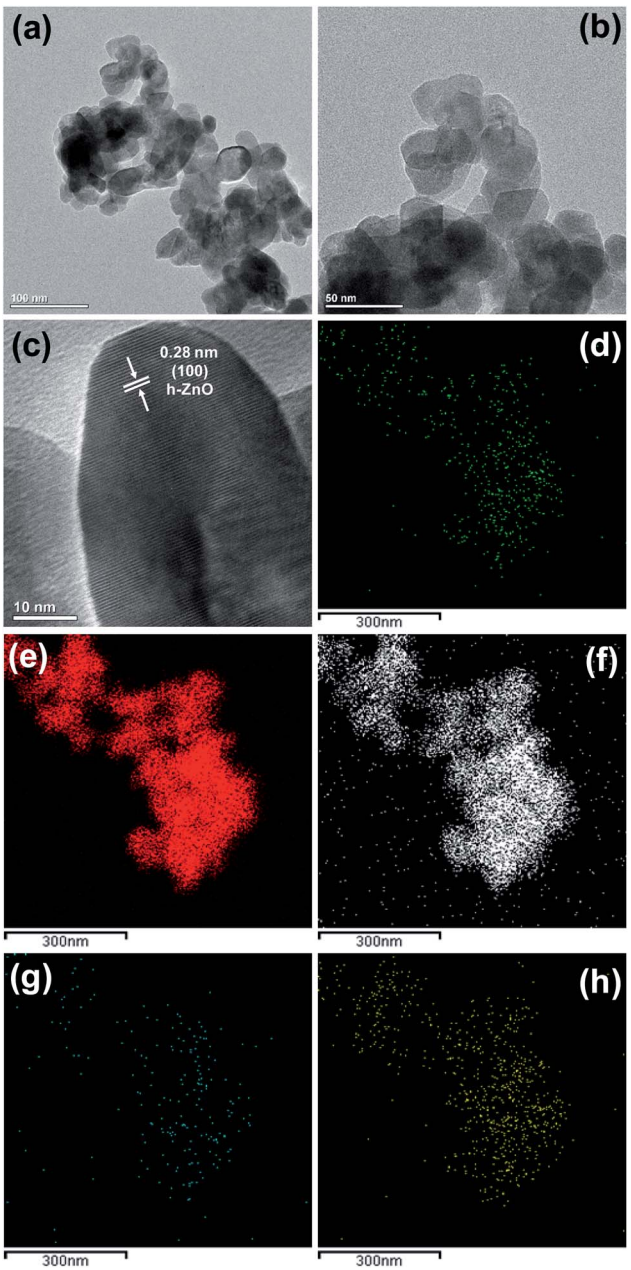

Fig. 2 (a, b) Transmission electron microscopy (TEM) images of the AZM nanocomposite, (c) corresponding high-resolution TEM image, and elemental mapping of (d) Ag, (e) Zn, (f) O, (g) Mo, and (h) S.

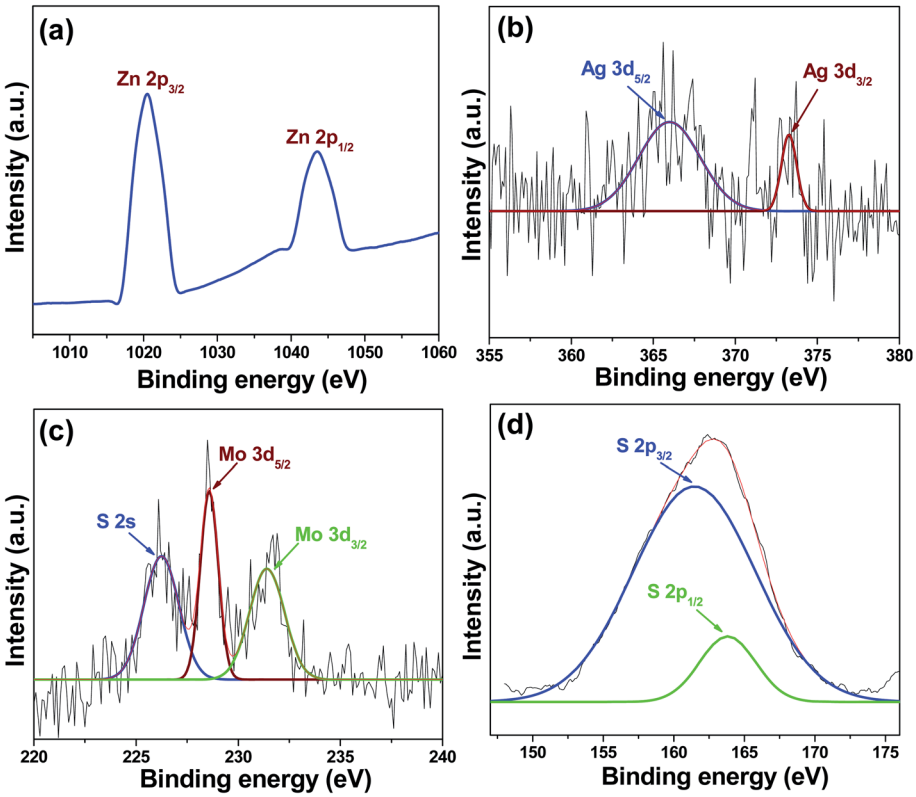

Fig. 3 X-ray photoelectron spectroscopy (XPS) results for the AZM nanocomposite: (a) Zn *2p* spectrum and Gaussian-fitted (b) Ag *3d*, (c) Mo *3d*, and (d) S *2p* spectra.

the ZO crystallite size in AZO indicated that Ag doping occurred. This reduction in crystallite size may also have implications for enhancing the antibacterial activity, as discussed later. Overall, the XRD results confirmed the successful preparation of the ZO, AZO, and AZM samples.

3.1.2. Morphology and microstructure. Fig. 2 shows the morphology and microstructure of a representative AZM

Table 1 Minimum inhibitory concentrations (MICs) of ZO, AZO, and AZM against multidrug-resistant (MDR) *E. coli*

			MIC (μg mL^{-1})		
Strain identification number[a]	Resistant antibiotics[b]	Genetic Features[c]	ZO	AZO	AZM
ATCC 25922	None	Type strain	500	62.5	62.5
CCARM 1011	AMP, CEP, GEN, NOR	bla_{AmpC}	250	62.5	31.25
CCARM 1013	AMP, CEP, GEN, NOR	bla_{AmpC}	250	62.5	31.25
CCARM 1368	AMP, CEP, CTX, GEN, NOR	bla_{ESBL}	250	250	125
CCARM1381	AMP, CEP, CTX, GEN, NOR	bla_{ESBL}	250	250	125
ATCC BAA-2452	ETP, IMP	bla_{NDM-1}	>250	125	31.25
ATCC BAA-2469	ETP, IMP	bla_{NDM-1}	>250	125	15.63
ATCC BAA-2471	ETP, IMP	bla_{NDM-1}	250	125	31.25
NCCP 16283	AMP, CAZ, CHL, CIP, COL, FEP, FOX, GEN, NAL, SXT, TET	*mcr-1*	250	250	125
NCCP 16284	AMC, AMP, CAZ, CHL, CIP, COL, DOR, ETP, FEP, FOX, IMP, MEM, NAL, SXT, TET	*mcr-1*; bla_{NDM-1}; bla_{TEM-1}, $bla_{CTX-M-27}$	250	250	125

[a] ATCC, CCARM, and NCCP represent American Type Culture Collection (https://www.atcc.org/), Culture Collection of Antimicrobial Resistant Microbes (HYPERLINK "http://knrrb.ccarm-bio.or.kr/index.jsp?rrb=ccarm" \o "http://knrrb.ccarm-bio.or.kr/index.jsp?rrb=ccarm"http://knrrb.ccarm-bio.or.kr/index.jsp?rrb = ccarm), and National Culture Collection for Pathogens (https://nccp.kdca.go.kr/), respectively. [b] Acronyms: AMC, Amoxicillin/Clavulanate (2 : 1); AMP, Ampicillin; CAZ, Ceftazidime; CEP, Cephalothin; CHL, Chloramphenicol; CIP, Ciprofloxacin; COL, Colistin; CTX, Cefotaxime; DOR, Doripenem; ETP, Ertapenem; FEP, Cefepime; FOX, Cefoxitin; GEN, Gentamicin; IMP, Imipenem; MEM, Meropenem; NAL, Nalidixic acid; NOR, Norfloxacin; TET, Tetracycline; SXT, Sulfamethoxazole-Trimethoprim. [c] *bla*, β-lactamase expressing gene; CTX-M-27: CTX-M β-lactamase detected in *E. coli* 27; ESBL: extended-spectrum β-lactamase; *mcr-1*: mobilized colistin resistance gene; NDM-1: New Delhi metallo-β-lactamase; TEM-1: a broad-spectrum β-lactamase.

sample. The TEM images of the AZM sample reveal quasi-spherical particles with sizes in the nanometer range (Fig. 2a and b). The high-resolution TEM image of the AZM sample (Fig. 2c) confirms the presence of ZO nanoparticles, as the distinct lattice fringes with an interplanar distance of 0.28 nm correspond to ZO (100) planes. Furthermore, elemental mapping of this sample revealed relatively uniform distributions of Ag (Fig. 2d), Zn (Fig. 2e), O (Fig. 2f), Mo (Fig. 2g), and S (Fig. 2h), consistent with the formation of the AZM nanocomposite. Hence, the TEM results for the AZM sample were consistent with the XRD results (Fig. 1) and confirmed the successful formation of the AZM nanocomposite.

3.1.3. XPS results. XPS analysis (Fig. 3) of the AZM sample was performed to determine the surface chemical composition and the chemical state of the elements.[7] In the Zn 2p spectrum (Fig. 3a), the two strong peaks at binding energies of 1021.2 and 1044.2 eV can be assigned to Zn $2p_{3/2}$ and Zn $2p_{1/2}$, respectively.[8] The energy difference between the Zn $2p_{3/2}$ and Zn $2p_{1/2}$ binding energies (~23.0 eV) corresponds to the Zn^{2+} valence state.[25] Ag doping of the ZO nanoparticles was confirmed by the Ag 3d spectrum (Fig. 3b), in which the two Gaussian-fitted peaks at 365.9 and 373.1 eV corresponded to Ag $3d_{5/2}$ and Ag $3d_{3/2}$, respectively. These values were consistent with those of metallic silver.[32] Gaussian fitting of the Mo 3d spectrum (Fig. 3c) revealed characteristic Mo peaks at 228.9 and 231.6 eV, which were assigned to Mo $3d_{5/2}$ and Mo $3d_{3/2}$, respectively.[24] An additional S 2s peak at 226.1 eV was also observed in the Mo region. Similarly, the S 2p spectrum exhibited peaks at 161.9 and 163.7 eV, corresponding to S $2p_{3/2}$ and S $2p_{1/2}$, respectively. Additionally, the atomic weight percentage (at%) of the components in the nanocomposite were obtained through the XPS analysis. The analysis has been made from the peak areas of the corresponding XPS signal for silver and zinc. From the XPS study, The contents (at%) of silver and Zn are found to be ~3.5% and Zn ~96.5%, respectively. Therefore, the obtained XPS data confirm the formation of an AZM nanocomposite, in good agreement with the XRD (Fig. 1) and TEM (Fig. 2) results.

3.2. Antibacterial activity

The antibacterial activities of ZO, AZO, and AZM were determined as MIC values (Table 1) against two different types of MDR *E. coli* strains expressing (1) cell-wall-active antibiotic-degrading β-lactamases encoded by bla_{AmpC}, $bla_{\text{TEM-1}}$/$bla_{CTX\text{-}M\text{-}27}$, bla_{ESBL}, and $bla_{NDM\text{-}1}$, and (2) a mobilized colistin resistance (*mcr-1*) gene product, which has recently become problematic. The MIC values of AZM against all the investigated *E. coli* cells were in the range of 15.63–125 μg mL^{-1}, indicating the AZM is 2- to 8-fold more active than AZO. AlamarBlue™ Cell Viability Reagent (Invitrogen, CA, USA), a ready-to-use resazurin (7-hydroxy-3*H*-phenoxazin-3-one 10-oxide)-based solution has been utilized in respect of determine the MIC clearly. As discussed in method section, when the reagent color is changed from blue to pink (Fig. S1†) it indicates the bacterial growth occurred, while no color change means bacterial growth was inhibited. The bactericidal activity of AZM was further confirmed by the non-

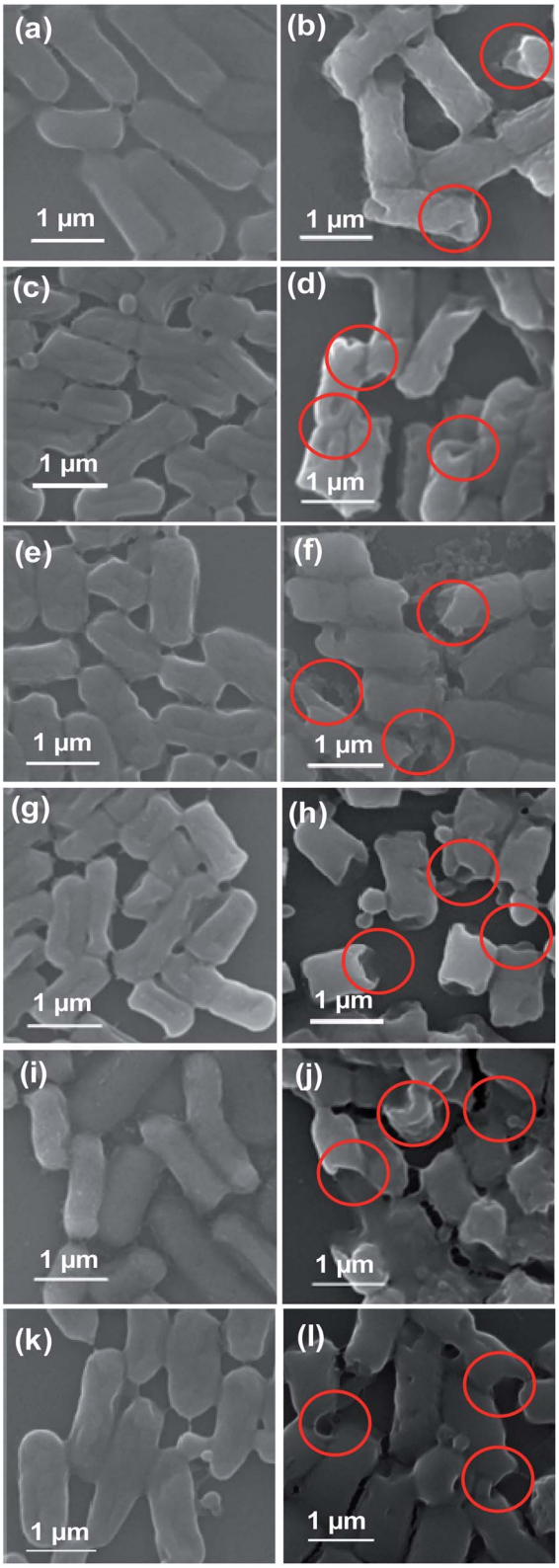

Fig. 4 Scanning electron microscopy (SEM) images of various *E. coli* strains (a, c, e, g, i, k) before and (b, d, f, h, j, l) after treatment with AZM at the sub-MIC level: (a, b) ATCC 25922, (c, d) CCARM 1011, (e, f) CCARM 1013, (g, h) ATCC BAA-2452, (i, j) ATCC BAA-2469, and (k, l) ATCC BAA-2471. Cell membrane disruption is indicated by red circles.

detection of viable cells from the fraction of ATCC BAA-2471 cells treated with samples at the MIC level on the agar plate (Fig. S2†). Among different types of antibiotic-resistant *E. coli* strains, those expressing β-lactamases had lower MIC values (6 of 8 tested strains: 75%) than MDR strains containing *mcr-1* gene. To determine whether the presence of β-lactamase encoding gene is the determinant for AZM activity, the MIC value was determined against a strain containing both bla_{NDM-1} and *mcr-1* genes (NCCP 16284). The presence of NDM-1 did not increase AZM activity, indicatng that the presence of the β-lactamase encoding gene itself is not a determinant for AZM activity, rather the *mcr-1* gene is likely a strong inhibitor of AZM activity. Therefore, the AZM nanocomposite is a promising nano-antibacterial agent for the selective disinfection of MDR *E. coli* strains producing β-lactamase.

3.3. Proposed antibacterial action mechanism of AZM

It has been reported that the antibacterial activity of NPs is primarily due to membrane damage caused by the adsorption of NPs on the cell walls, followed by penetration into the cell. To identify the antibacterial action mechanism of AZM nanocomposite, the morphologies of *E. coli* cells were analyzed using SEM with or without treatment by AZM nanocomposite at the sub-MIC (15.63 μg mL^{-1}) level, at which good antibacterial activity was observed. As shown in Fig. 4, the untreated bacteria cells have smooth surfaces without ruptures, and all cells in the population have similar sizes. However, treatment with the AZM nanocomposite caused the bacterial cells to rupture, resulting in morphological defects, such as smaller sizes than the non-treated cells and wrinkled membranes (as indicated by red circles in Fig. 4). Following AZM treatment, an increase in the population of smaller ruptured cells was observed, particularly in β-lactamase expressing MDR strains (Fig. 4h and j), suggesting that AZM preferentially targets such strains. Therefore, membrane damage is confirmed as a plausible mechanism for the antibacterial activity of AZM against cell-wall-active antibiotic-degrading MDR *E. coli* strains.

Further, we investigated whether any surface modification by AZM is additional mechanism of action. To this end, the role of surface charge of AZM, which might perturb the membrane structure, in the antibacterial activity was assessed by zeta-potential measurements at a range of concentrations corresponding to the MICs for different resistance type of MDR *E. coli* strains expressing either Mcr-1 or β-lactamase. As shown in Fig. 5a, the charge of AZM increased in a concentration-dependent manner, becoming positive at the MIC level (15.63 μg mL^{-1}: 2.35 mV to 125 μg mL^{-1}: 24.05 mV). *E. coli* is generally known to have a negative surface charge owing to the presence of negatively charged lipid A on the LPS component,[16] whereas the strain expressing Mcr-1 has a more positive surface charge owing to LPS remodeling by ArnT and EptA proteins.[33] Therefore, the positively charged AZM nanocomposite could neutralize negatively charged *E. coli*, ultimately paving the way for excellent antibacterial activity by charge neutralization mechanism. From the MIC results (Table 1), we hypothesized that cells with more negatively charged surfaces, such as β-lactamase expressing MDR strains of *E. coli*, will be more prone to interactions with positively charged AZM, which will aid in bacterial cell killing. In contrast, the positively charged strains expressing Mcr-1 will repulse AZM from the cell surface.

To confirm this hypothesis, we measured the zeta potential values of the representative MDR *E. coli* strains (BAA-2469 and NCCP 16283), which showed the highest and lowest activity against AZM. The zeta potential values were measured with and without treatment of AZM at the same concentration (7.8 μg mL^{-1}), which is the sublethal concentration of AZM against BAA-2469. As shown in Fig. 5b, both strains showed negative surface charges (−72.40 and −51.27 mV for BAA-2469 and NCCP 16283, respectively), confirming that the surface charge of the strain containing *mcr-1* gene product is less negative than that of the β-lactamase expressing strain. Correspondingly, in the presence of AZM, the net negative surface charge of BAA-2469 was remarkably reduced, indicating that the cells interacted with positively charged AZM. In contrast, the change in the zeta potential of NCCP 16283 was minimal, as its increased positive charge resulting from lipid modification inhibited its ability to interact with positively charged AZM. From these results, we conclude that membrane disruption through cell surface

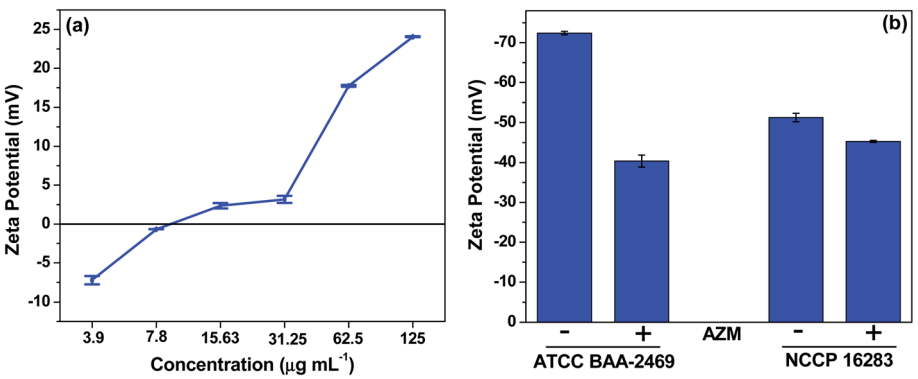

Fig. 5 Zeta potential measurements of (a) AZM at different concentrations and (b) ATCC BAA-2469 and NCCP 16283 *E. coli* cells before and after AZM treatment at the sublethal concentration (7.8 μg mL^{-1}). The data represent mean ($n = 3$) ± standard deviation ($p < 0.05$ indicates significant differences).

charge perturbation is the major mechanism of action for AZM in killing MDR *E. coli* strains, particularly those expressing β-lactamase.

4. Conclusions

In conclusion, an AZM nanocomposite was synthesized by immobilizing AZO NPs on MoS_2 nanosheets. The AZM nanocomposite outperformed the AZO nanoparticles as an antibacterial material against MDR *E. coli* strains by 2- to 8-fold with selectivity for those expressing β-lactamase. SEM analysis showed that AZM acted by disrupting cell membranes. Furthermore, zeta potential analysis revealed that the observed selectivity toward β-lactamase expressing MDR *E. coli* strains originated from enhanced interactions between this negatively charged strain and positively charged AZM at the MIC. This work shows that the combination of MoS_2 nanosheets with antibacterial metal oxide NPs provides a potential nanoantibiotic platform for fabricating antibacterial materials that can efficiently target β-lactamase expressing MDR *E. coli* strains.

Author contributions

Conceptualization, A. N. and K.-s. K.; Investigation, A. N. and J. S.; Formal analysis, A. N.; Writing, A. N. and K.-s. K.; Supervision, K.-s. K.; funding acquisition, K.-s. K. All authors have read and agreed to the published version of the manuscript.

Funding

This research was funded by a National Research Foundation of Korea (NRF) grant funded by the Korean government (MSIT) (grant number NRF-2021R1A2C1007413).

Conflicts of interest

There are no conflicts to declare.

Acknowledgements

The pathogen resources (NCCP No. 16283 and 16284) for this study were provided by the National Culture Collection for Pathogens (NCCP).

References

1 D. Cox, *Antibiotic resistance: the race to stop the silent tsunami facing modern medicine*, The Guardian. 2015 Aug 21, available from: http://www.theguardian.com/society/blog/2015/aug/21/antibiotic-resistance-the-race-to-stop-the-silent-tsunami-facing-modern-medicine.
2 H. I. Zgurskaya, C. A. Löpez and S. Gnanakaran, *ACS Infect. Dis.*, 2015, **1**(11), 512–522.
3 Z. Breijyeh, B. Jubeh and R. Karaman, *Molecules*, 2020, **25**(6), 1340.
4 J. H. Hewitt and J. Rigby, *J. Hyg.*, 1976, **77**(1), 129–139.
5 L. Poirel, J. Y. Madec, A. Lupo, A. K. Schink, N. Kieffer, P. Nordmann and S. Schwarz, *Microbiol. Spectrum*, 2018, **6**(4), ARBA-0026-2017.
6 *Antibiotic Resistance Threats in the United States*, 2019, available online: https://www.cdc.gov/drugresistance/biggest-threats.html, (accessed on 28 February 2022).
7 A. Naskar, S. Lee, Y. Lee, S. Kim and K. S. Kim, *Pharmaceutics*, 2020, **12**(9), 841.
8 A. Naskar, S. Lee and K. S. Kim, *Front. Bioeng. Biotechnol.*, 2020, **8**, 216.
9 M. Bhushan, S. Muthukamalam, S. Sudharani and A. K. Viswanath, *RSC Adv.*, 2015, **5**, 32006–32014.
10 K. V. P. Kumar, O. S. N. Ghosh, G. Balakrishnan, P. Thirugnanasambantham, S. K. Raghavan and A. K. Viswanath, *RSC Adv.*, 2015, **5**, 16815–16820.
11 M. Bhushan, Y. Kumar, L. Periyasamy and A. K. Viswanath, *Appl. Nanosci.*, 2018, **8**, 137–153.
12 M. Bhushan, Y. Kumar, L. Periyasamy and A. K. Viswanath, *Mater. Sci. Eng. C*, 2019, **96**, 66–76.
13 M. Bhushan, D. Mohapatra, Y. Kumar and A. K. Viswanath, *Mater. Sci. Eng. B*, 2021, **268**, 115119.
14 K. Tadyszak, J. K. Wychowaniec and J. Litowczenko, *Nanomaterials*, 2018, **8**(11), 944.
15 A. Naskar, H. Khan and S. Jana, *J. Sol-Gel Sci. Technol.*, 2018, **86**, 599–609.
16 H. Cho, A. Naskar, S. Lee, S. Kim and K. S. Kim, *Pharmaceutics*, 2021, **13**(2), 250.
17 A. Naskar and K. S. Kim, *Microb. Pathog.*, 2019, **137**, 103800.
18 Z. Wu, J. Qi, W. Wang, Z. Zeng and Q. He, *J. Mater. Chem. A*, 2021, **9**, 18793–18817.
19 A. Rai, H. C. P. Movva, A. Roy, D. Taneja, S. Chowdhury and S. K. Banerjee, *Crystals*, 2018, **8**(8), 316.
20 Y. Zhao, Y. Jia, J. Xu, L. Han, F. He and X. Jiang, *Chem. Commun.*, 2021, **57**(24), 2998–3001.
21 J. Li, J. Zheng, Y. Yu, Z. Su, L. Zhang and X. Chen, *Nanotechnology*, 2020, **31**(12), 125101.
22 S. Roy, A. Mondal, V. Yadav, A. Sarkar, R. Banerjee, P. Sanpui and A. Jaiswal, *ACS Appl. Bio Mater.*, 2019, **2**(7), 2738–2755.
23 S. R. Ali and M. De, *ACS Appl. Nano Mater.*, 2021, **4**(11), 12682–12689.
24 K. Kasinathan, K. Marimuthu, B. Murugesan, N. Pandiyan, B. Pandi, S. Mahalingam and B. Selvaraj, *J. Mol. Liq.*, 2021, **323**, 114631.
25 A. Naskar, S. Lee and K.-s. Kim, *RSC Adv.*, 2020, **10**, 1232–1242.
26 R. S. Kumar, S. H. S. Dananjaya, M. D. Zoysa and M. Yang, *RSC Adv.*, 2016, **6**, 108468–108476.
27 H. B. Dias, M. I. B. Bernardi, V. S. Marangoni, A. C. de Abreu Bernardi, A. N. de Souza Rastelli and A. C. Hernandes, *Mater. Sci. Eng., C*, 2019, **96**, 391–401.
28 C. Karunakaran, V. Rajeswari and P. Gomathisankar, *Mater. Sci. Semicond. Process.*, 2011, **14**, 133–138.
29 G. Iqbal, S. Faisal, S. Khan, D. F. Shams and A. Nadhman, *J. Photochem. Photobiol., B*, 2019, **192**, 141–146.
30 T. I. Kim, B. Kwon, J. Yoon, I. J. Park, G. S. Bang, Y. Park, Y. S. Seo and S. Y. Choi, *ACS Appl. Mater. Interfaces*, 2017, **9**(9), 7908–7917.

31 Y. Qi, N. Wang, Q. Xu, H. Li, P. Zhou, X. Lu and G. Zhao, *Chem. Commun.*, 2015, **51**, 6726–6729.
32 A. Kaur, A. O. Ibhadon and S. K. Kansal, *J. Mater. Sci.*, 2017, **52**, 5256–5267.
33 S. M. Zimmerman, A.-A. J. Lafontaine, C. M. Herrera, A. B. Mclean and M. S. Tren, *Antimicrob. Agents Chemother.*, 2020, **64**, e01677-19.